

Modified SDOF Models for Improved Representation of the Impact Response of Composite Plates

PAOLO FERABOLI*

*Department of Aeronautics and Astronautics, University of Washington
Box 352400 Seattle, WA 98195-2400, USA*

(Received August 20, 2005)

(Accepted November 11, 2005)

ABSTRACT: Previous research has shown that simple single degree of freedom (SDOF) models can be used successfully to reproduce the force–time response of composite plates subjected to low-velocity impacts (LVI). In particular, a simple spring–mass (SM) model yields accurate estimates of the peak contact force as a function of impact energy. The major limitation of this model is that it applies only to elastic impact events, and ceases to be valid after the onset of damage. The effort of this investigation is to modify the SM model, while retaining the simplicity of its formulation, and to extend its range of validity to the super-critical regime. Three models are derived, namely the damaged stiffness, the dissipated energy, and the spring–mass–dashpot models, and their validity is examined through comparisons with experimental data. Impact force–time traces for carbon/epoxy laminates exhibiting various combinations of laminate thickness and support span are collected, and it is found that the additional unknowns introduced for each of the models, although determined empirically, are strongly related to the structural parameters for each configuration investigated.

KEY WORDS: impact modeling, impact testing, damage resistance, progressive damage.

INTRODUCTION

Background

HISTORICALLY, THE FIRST impact tests performed on composite materials for aerospace applications were noninstrumented [1,2]. The target laminates or structures were impacted at a nominal impact energy level, and the subsequent damage was measured with destructive and nondestructive inspection methods. Eventually, the

*E-mail: feraboli@aa.washington.edu

Figures 1–5 and 8–13 appear in color online: <http://jcm.sagepub.com>

goal of the test was to inflict impact damage to the structure, for certification purposes, and then to measure the residual properties of the panel. This practice originated the tradition to build the so-called damage maps, which relate a measure of damage (such as dent depth or projected delamination area) to incident kinetic energy, as well as the compression after impact (CAI) curves, where the residual compressive strength of the panel is plotted against the incident kinetic energy. Later developments, which coincided with the commercialization of instrumented impact devices [3–5], indicated an advantage in the use of dynamic load-cells. The use of an instrumented drop tower such as the General Research Corporation (GRC) Dynatup[®] enables the recording of force and time, which are directly measured, as well as energy, deflection and velocity, which are calculated. In conventional experimental setups [3–11] a flat composite plate is subjected to an out-of-plane, concentrated load by means of a falling weight and it is possible to characterize the panel's elastic behavior, failure initiation, and failure propagation in terms of applied dynamic force and energy.

In order to facilitate the understanding of these concepts, a brief summary of the terminology used is reported:

- Impact energy – incident kinetic energy of the impactor,
- Peak force – maximum recorded force,
- Critical force – value of the force at which a first change in out-of-plane stiffness of the material occurs, also denoted as delamination threshold,
- Critical energy – value of the impact energy corresponding to the critical force,
- Dissipated energy – amount of energy absorbed mainly in damage mechanisms but also in other nonconservative phenomena (i.e., vibrations, friction, specimen/fixture slipping) and therefore, not restituted to the rebounding impactor,
- Total contact duration – resident time of the impactor on the target,
- Sub-critical (or elastic) impact events – range of impact energy values below damage threshold,
- Super-critical impact events – range of impact energy values above threshold.

Here, failure is defined as a sharp drop (clearly visible) in the force–time curve, corresponding to damage initiation, either in the ply plane or at the interface of two adjacent plies. The nature of in-plane failure is matrix cracking, splitting, or fiber breakage, while the nature of interply failure is delamination induced by interlaminar shear.

Experimental Setup

The analytical equations derived in the following paragraphs are validated with the results of impact tests performed on AS4/NCT301 laminates, having $[0/90/\pm 45]_n$ layup, with $n=2-5$ [6]. A total of five structural configurations (summarized in Table 1) are tested, by varying aperture span and laminate thickness. The reference configuration C1 is a 32 ply ($n=4$) laminate with nominal thickness of 0.145 in. (3.68 mm), supported over a 2.5 in. diameter circular aperture. The fixture is comprised of two steel plates having a circular aperture of two different sizes, which are clamped together by four screws located at the periphery of the composite target. The composite plate is situated between the two steel plates and is positioned over the aperture with the aid of three locating pins. The four screws are then tightened to provide (partially) clamped boundary conditions.

Table 1. Summary of experimental setup.

Configuration	Number of plies	Nominal thickness (mm)	Aperture diameter (mm)
C1	32	0.145 (3.68)	2.5 (63.50)
C2	32	0.145 (3.68)	5.0 (127.0)
C3	16	0.072 (1.83)	2.5 (63.50)
C4	24	0.108 (2.74)	2.5 (63.50)
C5	40	0.181 (4.60)	2.5 (63.50)

The instrumented drop tower is a GRC Dynatup[®] model 8250, and the software used for data recording/analysis is the 930 version. Impactor carriage weight is 9.92 lbs (4.51 kg), and the striker, or tup, is a 6061-T6 aluminum cylinder with a 1.5 in. (38.1 mm) diameter hemispherical end.

ELASTIC RESPONSE AND DAMAGE INITIATION

Sub-critical Regime

A force–time trace is the typical tool used to interpret data from instrumented impact tests (Figure 1). The onset of specimen-indenter contact is noted by the detection of a non-zero contact force: as the indenter presses into the specimen, the contact force increases. A sub-critical test, which is ‘purely’ elastic in nature, can be represented by a half sine wave, if the ratio of impactor to target mass is sufficiently high [6]. Using a spring–mass model [12]:

$$m\ddot{x} + K_0x = 0 \quad (1)$$

where m indicates impactor mass, x is the transverse displacement of the carriage (which is assumed to coincide with the target, hence assuming that there is no significant permanent indentation), and K_0 is the pristine (undamaged) structural stiffness, and setting the instantaneous value of the contact force $P = -m\ddot{x}$, it is possible to obtain the known sine function:

$$x = V \sqrt{\frac{m}{K_0}} \sin\left(\sqrt{\frac{K_0}{m}} t_c\right) \quad (2)$$

where V is the impact velocity and t_c the total contact duration.

Provided that the system behaves in an elastic fashion, and the assumption of sine wave is correct, the total contact duration of the impact event is a direct indication of the effective structural stiffness of the target, and is independent of the impact energy level at which the test is performed [3,6]:

$$t_c = \pi \sqrt{\frac{m}{K_0}} \quad (3)$$

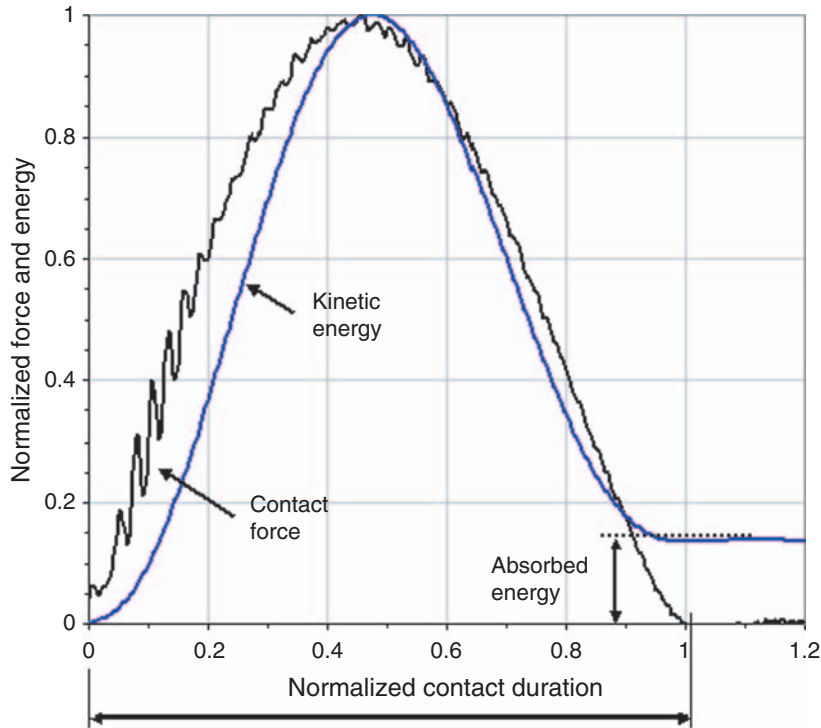


Figure 1. Representative contact force and kinetic energy vs time history for a low-energy elastic test.

Employing a simple energy balance, under the assumption of linear elastic response, the data for the peak force can then be accurately fitted by a well-accepted power law curve [12]:

$$P_{SM}^{\text{peak}} = \sqrt{2K_0 E_i} \quad (4)$$

where E_i is the impact energy, and P_{SM}^{peak} is the theoretical value of the peak contact force. The peak force is therefore directly related to the effective stiffness of the structure, as is the total contact duration, but it is also strictly dependent on incident kinetic energy, even for an elastic impact test. It has therefore been suggested that using peak contact force as the sole governing parameter may lead to ambiguous results when comparing the impact performance of different composite panels [6]. For the same reason, instrumented ‘coin-tap’ test devices [13], which are portable impulse hammers, employ contact duration rather than peak force to detect the presence of damage within a structure during aircraft inspection.

The signal generated and recorded by the data acquisition system (Figure 1) is a complex combination of the true mechanical response of the specimen, inertial loading of the tup, and low-frequency fluctuations [3]. The first component is the obvious objective of the investigation, yet often the second and third components can overshadow the real results. In particular, the inertial loading is the force caused by rigid body acceleration of the specimen from a rest position to the velocity of the impacting assembly, and it generally

dominates the top signal for the first 10–100 μs . On the other hand, the low-frequency fluctuations typical of impact tests are superimposed oscillations primarily caused by stored elastic energy and inertial effects. The force–time signal is therefore not necessarily indicative of the reaction of the specimen, and the importance of understanding the significance of these phenomena lies in the fact that the operator or the automated data analysis routine (as the Dynatup[®] 930 software) may incorrectly select the value of the peak force if the inertial peak or any of the following oscillations is the highest load value recorded. Since the oscillations, also referred to as ringing, are harmonic about the mean or true signal value, the peak force data can potentially be incorrect.

The energy–time curve is customarily presented in the same plot as the force–time curve (Figure 1). In an ideal setup, the energy curve would peak at the same time as the force curve, which is theoretically reached when the velocity of the impactor approaches zero at the point of maximum deflection. In reality, however, instrumentation errors introduce a slight delay in the signal and the curve peaks effectively a few microseconds after the force–time curve. At the end of contact, part of the incident kinetic energy has been dissipated, even in an elastic test, in non-conservative phenomena, e.g., as friction along the rails and slipping at the boundaries. The energy balance that relates impact energy (E_i) to the elastic strain energy (E_E) is also comprised of the non-conservative term (E_{NC}) and the dissipated energy term (E_D) [14], associated with the damage creation and propagation:

$$E_i = E_E + E_{NC} + E_D. \quad (5)$$

For each impact test, the peak contact force is recorded and plotted against the incident kinetic energy, and the results are reported in a force–energy plot such as the one in Figure 2 for reference configuration C1. The curve to the left of the damage threshold value is the sub-critical regime. In this region, the peak force recorded during an elastic impact test varies according to Equation (4) if a simple spring–mass (SM) model is used. Similarly, the energy dissipated during an impact event can be plotted against the incident kinetic energy, as in Figure 3. Again, the region to the left of the damage threshold is the sub-critical regime, and it can be seen that even in this regime the energy dissipated is non-zero, as mentioned earlier.

Super-critical Regime

If the impact energy level at which the test is conducted is sufficiently high, the damage threshold is exceeded and the event falls in the super-critical regime. For impact energies just above the critical level, the force–time trace has the appearance of curve A in Figure 4. In this curve, the contact force increases up to the point of failure, then suddenly drops, and is followed by the onset of the low-frequency oscillations in the signal mentioned before. Eventually load picks up again, but it never reaches the same value as the one where failure initiated, hence critical and peak forces coincide. The onset of damage is associated to a specific value of contact force and kinetic energy, and this value remains constant throughout the entire supercritical regime, independently of the impact energy level. For greater impact energies, as in the case of curve B in Figure 4, the impactor has sufficient momentum to reach a greater value of contact force after initiating damage. Therefore, critical and peak forces do not coincide. Eventually, when the kinetic energy

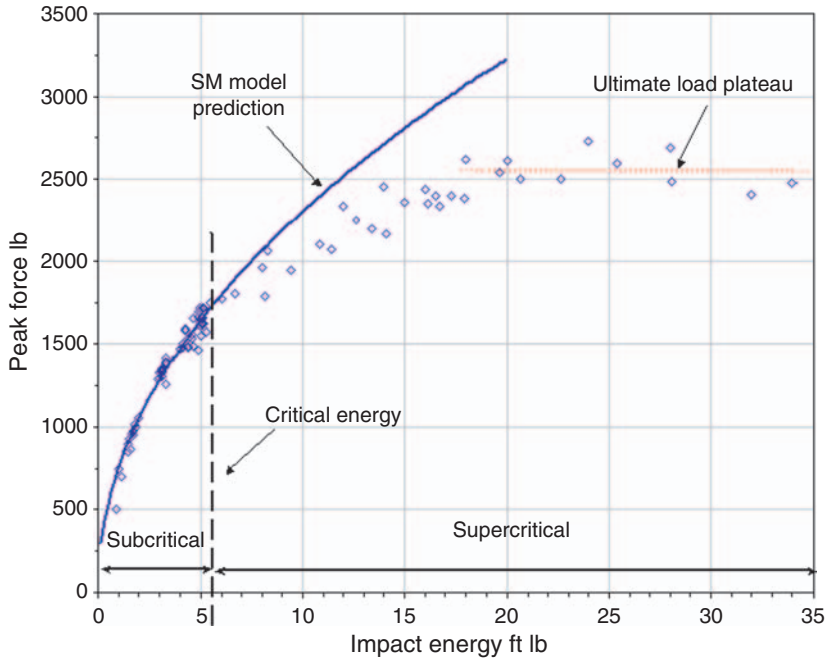


Figure 2. Peak impact force plot, highlighting the damage threshold, and sub- and super-critical regimes.

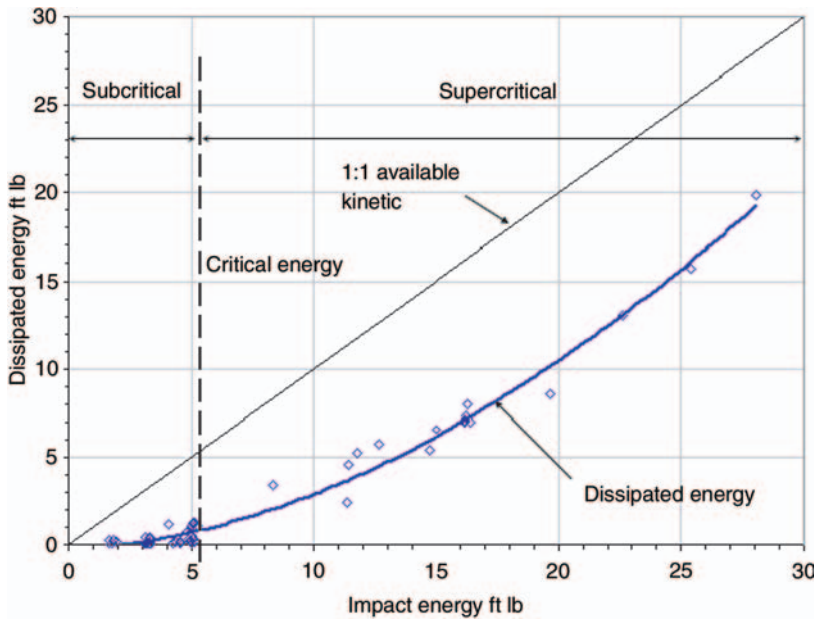


Figure 3. Dissipated energy plot, highlighting the damage threshold, and sub- and super-critical regimes.

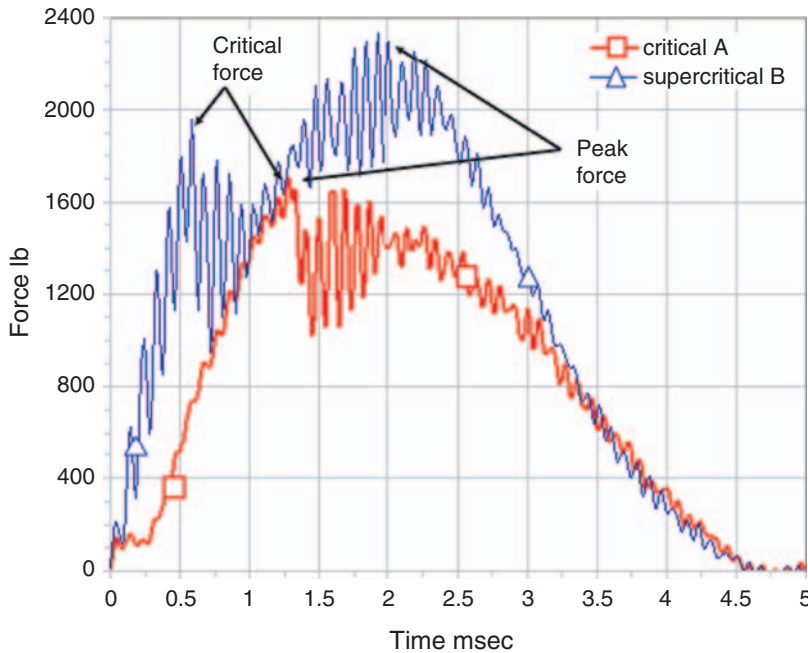


Figure 4. Representative contact force profiles for two damage-inducing impact events, also showing inertial and harmonic oscillations.

reaches the maximum load bearing capability of the plate, the value of the peak force ceases to increase, and it remains constant around a mean ultimate dynamic load. For strain-rate insensitive materials, such as modern carbon/epoxy systems, this value has been shown to coincide with the mean static ultimate load [6–8]. In the supercritical regime, the value of peak force recorded in a super-critical event is however quite lower than the one predicted by the spring–mass model for the same level of impact energy (Figure 2). The discrepancy between the experimental results and Equation (4) progressively intensifies after the damage threshold is exceeded and, most notably, it increases unboundedly once the dynamic plateau is reached. The error in which a user may incur, if not aware of this complex behavior is demonstrated by Figure 5(a), from Hinrichs et al. [15]. This plot emphasizes the discrepancy in the measured versus the predicted response, and which the authors suspected to be associated to the creation and propagation of damage. The symbols represent the different values of panel thickness tested. Re-plotting the peak force data against the nominal impact energy (Figure 5(b)) shows that the majority of the tests conducted effectively falls in the region of dynamic plateau. Inconsistent trends are also reported by Nettles and Douglas [9] for the projected delamination area using peak force as the damage metric. In this case as well the tests are conducted in the region of the dynamic plateau, where if the impact energy increases, the damage size also increases but the peak force remains constant [6].

On the other hand, a plot of the energy dissipated in the creation and propagation of damage (Figure 3) shows a monotonic, nearly quadratic increase with available kinetic energy (1:1 straight line). It is well accepted in the literature [6] that, absorbed energy can be a very useful tool to assess the extent of damage in the laminate, provided that an

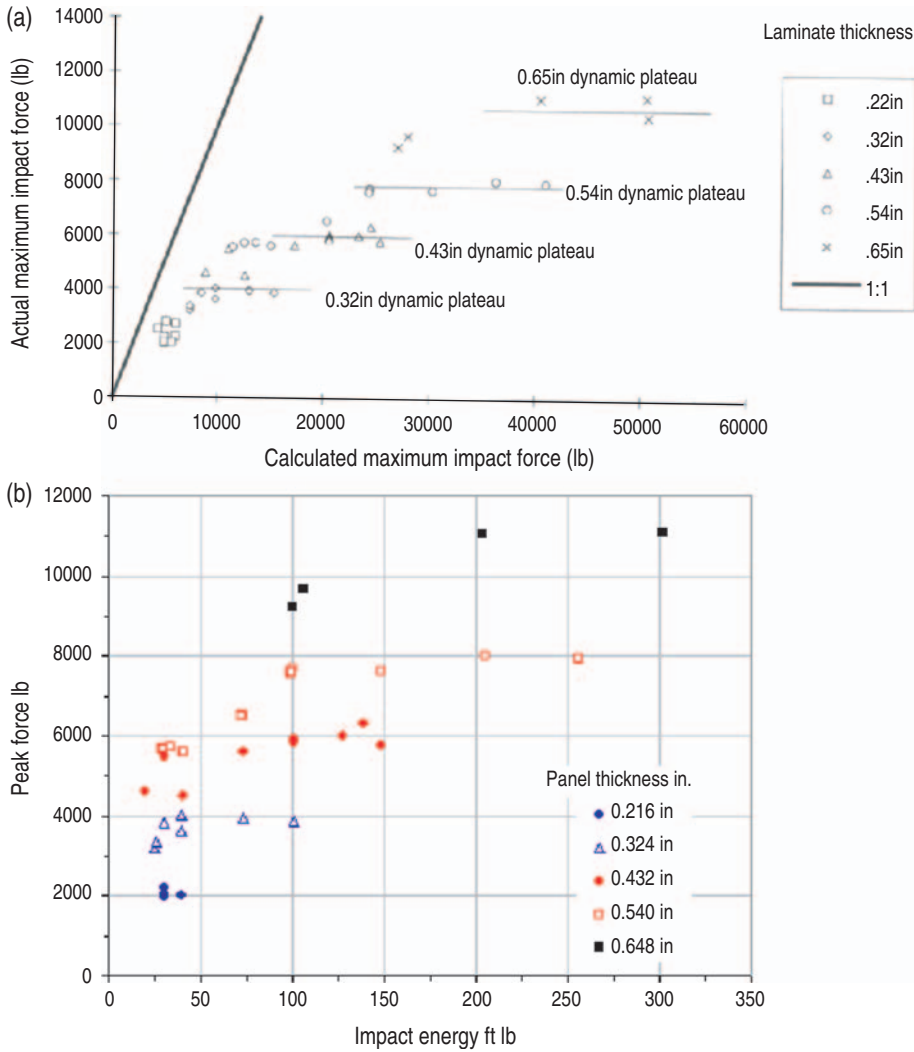


Figure 5. (a) Discrepancy between predicted and measured peak force data, from [15] and (b) re-plot of the measured peak force data of Figure 5(a) against impact energy, showing that the majority of the data points lie in the dynamic plateau.

understanding of the losses in the elastic regime is available. While current Federal Aviation Administration (FAA) damage tolerance certification efforts still rely on impact energy-based rather than force-based criteria [2], the use of an instrumented device, and hence of contact force, undoubtedly presents numerous advantages for gaining more in-depth understanding of the impact response of composite panels. For that reason, a reliable tool is required to predict the value of contact force at failure, but also the value of peak contact force. The following section describes the methods by which Equation (4) can be modified to account for the discrepancy on the value of peak force between the prediction and the experimental data, while retaining at the same time the simplicity of a single degree of freedom (SDOF) model.

MODIFIED SDOF MODELS

Previous Research

Abrate [12] provides a complete formulation of the spring–mass model for the elastic system of a projectile impacting a plate (Figure 6(a)). The model includes the effective structural stiffness of the target, which is represented by the two linear bending and shear springs in series (K_b and K_s), and the nonlinear membrane and contact stiffness springs (K_m and K):

$$M_2\ddot{x}_2 + K_{bs}x_2 + K_mx_2^3 + K(x_1 - x_2)^\alpha = 0 \quad (6)$$

where M_2 is the mass of the target, x_2 is the transverse displacement of the target and its temporal derivatives, x_1 is the transverse displacement of the tup, and α is the nonlinear indentation exponent. If the membrane effects are negligible and the indentation component is not significant, the system can be linearized to the one of Figure 6(b), which leads to the Equation (4). While Equation (6) refers to a purely elastic response, which means that it can be used only up to the damage threshold, Olsson et al. [16] report that Equation (6) can be used to predict the force required for damage initiation. The golf industry has used various spring–mass–dashpot (SMD) models extensively and successfully to capture the highly nonlinear response of the viscous golf ball. Evolutions of simpler models continue to appear, and the resulting predictions become progressively more accurate. The Simon model [17] can be written as:

$$m\ddot{x} + C\dot{x} + kx^{3/2} = 0 \quad (7)$$

where, $C = (k\alpha x^{3/2})$. The k and α coefficients have to be determined by experimental data fitting. Johnson and Lieberman [17] suggest a modified nonlinear model that includes a β exponent, which captures the impact velocity-dependent effects observed experimentally on the visco-elastic material:

$$m\ddot{x} + C\dot{x}^\beta + kx^{3/2} = 0. \quad (8)$$

The nondimensional exponent β , obtained by experimental fitting of golf ball impact data, has a value within the range 1.25–1.50, close to the theoretical value of 3/2 for an elastic impact between a sphere and a flat barrier [18]. Cochran [19] combines a linear SMD model for the plate with a nonlinear SMD for the ball, thereby obtaining a contact force proportional to the 3/2 exponent of the displacement, as predicted for small deformations of a sphere [18]:

$$m\ddot{x} + c\dot{x}|\dot{x}|^{1/2} + kx|x|^{1/2} = 0 \quad (9)$$

where m is the mass of the ball, and c and k have now units of $(\text{N/m})^{3/2}$ and $(\text{N s/m})^{3/2}$. A modification of the SM model is suggested by Gong and Lam [20] to include the effects of structural damping on the transient response of laminated plates. A finite element (FE) approach is implemented using a two-layer beam geometry for the target, comprised of a

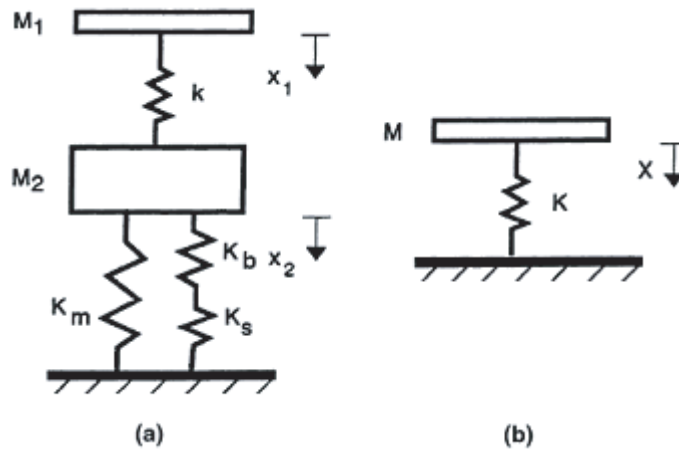


Figure 6. (a) Complete spring-mass model that includes bending, shear, membrane, and indentation stiffness springs and (b) linearized sdof model [12].

basic elastic layer (1) and damping layer (2), which are modeled as a spring-mass-damper system:

$$m_1 \ddot{x}_1 + \frac{\eta_{st} K_1}{\omega_{11}} \dot{x}_1 + (K_1 + K_2)x_1 - K_2 x_2 = 0 \quad (10)$$

where x is the transverse displacement, η_{st} is the effective structural loss factor, ω_{11} is the fundamental frequency of the two-layered panel, K_1 is the equivalent stiffness of the panel, and K_2 the effective contact stiffness. Satisfactory results are obtained with this approach, but the method suffers from the necessity of using FE codes for the expensive computational effort required. A FE model is integrated by Tomblin et al. [10,11] with experimentally determined contact laws to predict the impact response of sandwich panels. These laws, determined from indentation tests on rigid base, are characterized by an initial elastic region up to a critical value of the indentation depth, which is followed by a nonlinear, inelastic region up to facesheet fracture.

$$\begin{aligned} P_{0-cr} &= C_0 u \\ P_{cr-fract} &= C_1 + C_2 u^{C_3} \end{aligned} \quad (11)$$

where the C coefficients are obtained by curve fitting of the experimental data, and are a function of skin and core properties. The energy dissipated in contact deformation is the area enclosed between the loading and unloading portion of the curve. If the contact laws are linearized in both the loading (K_L) and unloading (K_{UL}) phases, the energy dissipated is simply a function of the ratio K_L/K_{UL} . The model can thus be used to predict the energy dissipated during the impact event in damage initiation and propagation. This type of empirical formulation, which requires extensive correlation of coupon-level test data to simplified analytical or numerical models, is typical of certification-oriented programs. Anderson [21] successfully introduces energy-absorbing elements to account for material damage in thin sandwich laminates. Impact energy is thus dissipated through the use of velocity-proportional or displacement-proportional dampers, or using a

complex stiffness formulation. Unfortunate attempts are initially made using a velocity-proportional damper in parallel with a nonlinear spring (Voigt element):

$$m\ddot{x} + c_v^V \dot{x} + kx^n = 0 \quad (12)$$

and using a displacement proportional damper:

$$m\ddot{x} + c_d x + kx^n = 0. \quad (13)$$

In the preceding equations, m is the target mass, c is the velocity or displacement proportional damper, k the effective bending stiffness, and n an empirical exponent greater than 1. However, both approaches prove to be inaccurate when compared to experimental results due to the initial velocity requirements on the system, which result in a nonzero contact force (Equation 7), and to an apparent lack of sensitivity to displacement variations (Equation 8). A partial success is achieved using complex stiffness damping:

$$m\ddot{x} + k_i(1 + i\eta)x = 0 \quad (14)$$

where k is a linearized stiffness, and η is an empirically determined damping coefficient, but both real and imaginary components are not of easy determination. Ultimately, he reports achieving the most satisfactory results with a velocity-proportional damper in series with the nonlinear spring (Maxwell element). Since now both displacement and force traces are to be determined, the model has effectively two degrees of freedom (TDOF), and becomes computationally more expensive:

$$m\ddot{x} + c_v^M \dot{x} - \frac{c_v^M (F/k)^{1/n} \dot{F}}{nF} = 0 \quad (15)$$

where F is the contact force and its time derivative, and the other symbols are the same as in the previous equations. Hoo Fatt and Park [22] employ a nonlinear spring $P(x)$, which represents the indentation behavior of the facesheet on a rigid foundation, and a constant-force dashpot Q_d , which represents the dynamic crushing resistance of the core:

$$m\ddot{x} + P(x) + Q_d = 0. \quad (16)$$

The solution for the peak force P_{\max} is obtained by numerical integration and is a complex function of impactor mass, impactor velocity, and global and local stiffness.

In the previous section, it was shown that Equation (4) successfully estimates the value of the peak contact force for linear elastic systems, but progressively overestimates the experimental results for increasing impact energies beyond the damage threshold (Figure 2). This phenomenon can be seen also in Figure 8 where, for a supercritical impact energy level, Equation (4) predicts a half-sine force-time curve (denoted as K_0 model). The K_0 model predicts a higher peak force and shorter contact duration than the one measured experimentally; however, the agreement is excellent up to the point of failure, which occurs at time t_f . After failure, the two traces begin to diverge, and the discrepancy in the peak force, which occurs at time t_M , is attributable to the lower value of the effective

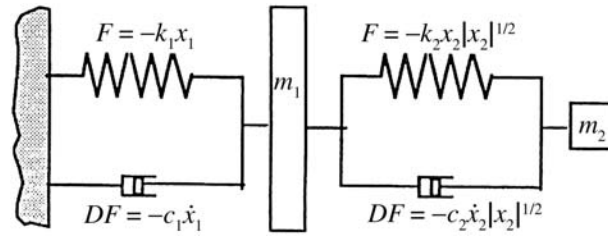


Figure 7. The response of the target/impactor system is modeled as a linear model of the target in series with a nonlinear model of the impactor [19].

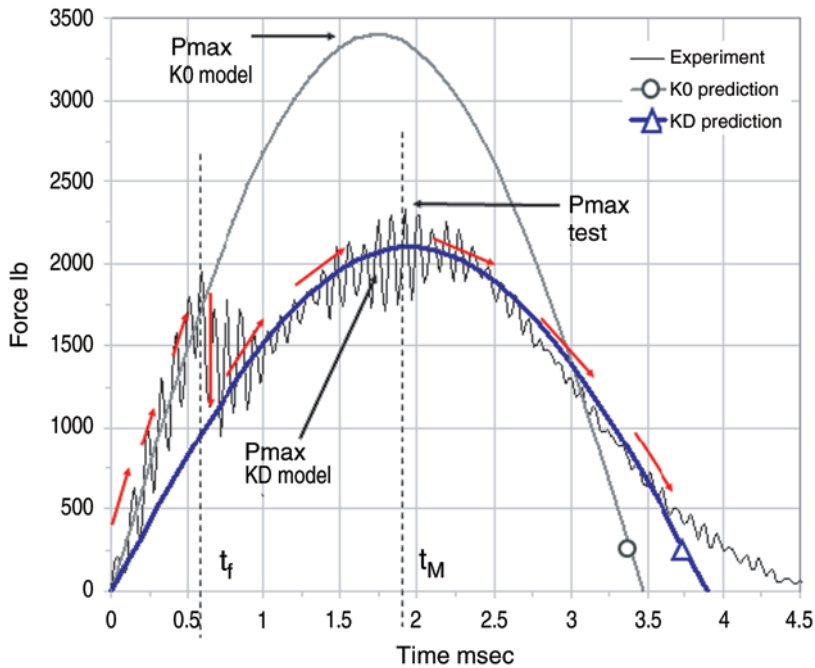


Figure 8. Example of force–time trace highlighting the discrepancy between the prediction of the SM model, the experimental data, and the accuracy of the damaged stiffness model.

structural stiffness. If a similar SM model with a lower stiffness value (K_D model) is used, the agreement becomes excellent from the point of failure on.

The great advantage of these SDOF models is their simplicity, and they require modest empirical correlation. In order to maintain the simple formulation of Equation (4) while capturing the dynamic response associated to the presence of damage, it may be possible to proceed in two directions. Retaining the SM model leading to Equation (4), the only two parameters that can be modified are the effective structural stiffness K_0 and the available impact energy E_i . In the following paragraphs, two modifications of Equation (4) containing one additional unknown related to the state of damage are developed, and are referred to as ‘damaged stiffness’ (K_D) and ‘dissipated energy’ (E_D), model respectively. If, however, an approach similar to Equations (7–9, 12, 13, 16) is pursued, a SMD model can be employed. The model captures the dynamic response of the damaged panel by

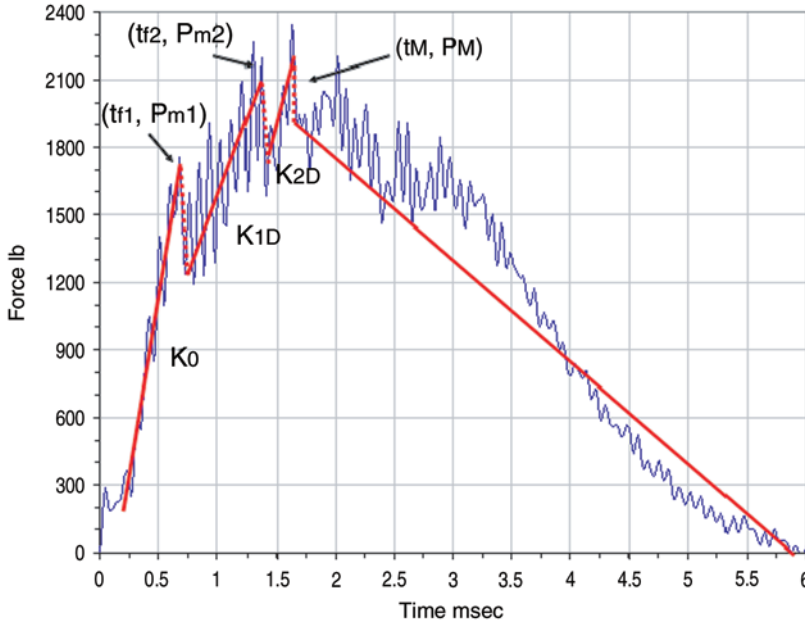


Figure 9. Super-critical force vs time history highlighting the different regions of instantaneous damaged stiffness.

means of a nonlinear viscous damper proportional to the impact velocity, which is characterized by two additional unknowns.

Damaged Stiffness (K_D) Model

For a supercritical impact (Figure 9), the force–time trace presents at first a sharp drop in correspondence of the point of failure initiation, which is indicated by a sudden decrease in the transverse stiffness of the plate [4,6]. After the drop, the contact force increases further (provided that the impactor has enough kinetic energy), but the slope of the curve is somewhat lower than in the earlier region due to the lower stiffness of the target. Other more or less distinct drops can be seen in the force–time trace, corresponding to other points of failure in the material. Each of these points (j th) can be described by a pair (t_{fj}, P_{mj}) of peak force and time, and the value of the instantaneous structural stiffness for that portion of the trace can be denoted as $K_{(j-1)D}$. For example, first failure occurs at (t_{f1}, P_{m1}) , and the effective structural stiffness up to that point is K_0 (pristine or undamaged value). It is therefore possible to account for the progressive change in transverse stiffness, associated with the instantaneous state of damage within the panel, throughout the entire impact event. A modification of Equation (4) that accounts for the effective instantaneous structural stiffness can be written as:

$$P_{KD}^{peak} = \sqrt{2 \left[K_0 \left(\frac{t_{f1}}{t_M} \right) + K_{1D} \left(\frac{t_{f2} - t_{f1}}{t_M} \right) + K_{(j-1)D} \left(\frac{t_{fj} - t_{j-1}}{t_M} \right) + \dots + K_{(M-1)D} \left(\frac{t_M - t_{M-1}}{t_M} \right) \right]} E_i \tag{17}$$

where $M-1$ is the total number of drops in the force–time curve up to the point of peak force (t_M). Since peak force is reached at the peak of the force–time curve, where the impactor arrests its fall and begins to reverse its motion, only the loading part of the curve is of interest in the prediction of peak force, and it is fair to normalize the time to failure with respect to the time to peak force. This ratio is a nondimensional term, having values between zero and unity, which is indicative of how much of the loading curve undergoes the impact event at a prescribed value of the structural stiffness. It is worth noticing that for a purely elastic or purely critical event, where peak force is reached exactly at the apex of the force–time curve, time-to-failure equals time-to-peak-force, hence Equation (17) reduces to Equation (4). To give an example of how the modified model can be applied, it is possible to consider the supercritical event of Figure 9. There appear to be at least two large drops in the curve before peak force is reached, hence:

$$P_{KD}^{\text{peak}} = \sqrt{2 \left[K_0 \left(\frac{t_{f1}}{t_M} \right) + K_{1D} \left(\frac{t_{f2} - t_{f1}}{t_M} \right) + K_{2D} \left(\frac{t_M - t_{f2}}{t_M} \right) \right] E_i}. \quad (18)$$

Since $t_{f1} = 0.675$ m s, $t_{f2} = 1.375$ m s, and $t_M = 1.637$ m s, the three nondimensional terms become:

$$P_{KD}^{\text{peak}} = \sqrt{2 [K_0(0.412) + K_{1D}(0.428) + K_{2D}(0.160)] E_i}. \quad (19)$$

It can be easily seen that the three time-ratios add up to unity, or 100%. The great advantage of this type of approach is that it retains the simple formulation of a SDOF model, and it is valid in the entire range of impact energy levels. With respect to the elastic SM model, this approach requires only additional information regarding K_{jD} , which has to be determined empirically. However, this type of approach can yield extremely accurate results (Figure 10, Equation (17)) and lends itself to practical implementation into a progressive failure analysis (PFA) and FE code.

Dissipated Energy (E_D) Model

It has been noted that the majority of the energy absorbed during an impact event is dissipated in the initiation and propagation of damage [14]. This energy increases in a nearly quadratic fashion with increasing available impact energy (Figure 3):

$$E_D \propto E_i^p \propto V^{2p} \quad (20)$$

where V is the impact velocity, and $p = (1.25-2.0)$. It is thus fair to assume that the state of damage within the panel is proportional to the impact velocity elevated to an exponent comprised between 2.5 and 4.0. Nevertheless, the portion of incoming kinetic energy that is absorbed in matrix damage, delamination origination, and fiber breakage does not contribute to the panel's dynamic structural response. The initiation and propagation of damage has the effect of reducing the amount of energy available for reaching the theoretical value of peak force. Leaving the effective structural stiffness

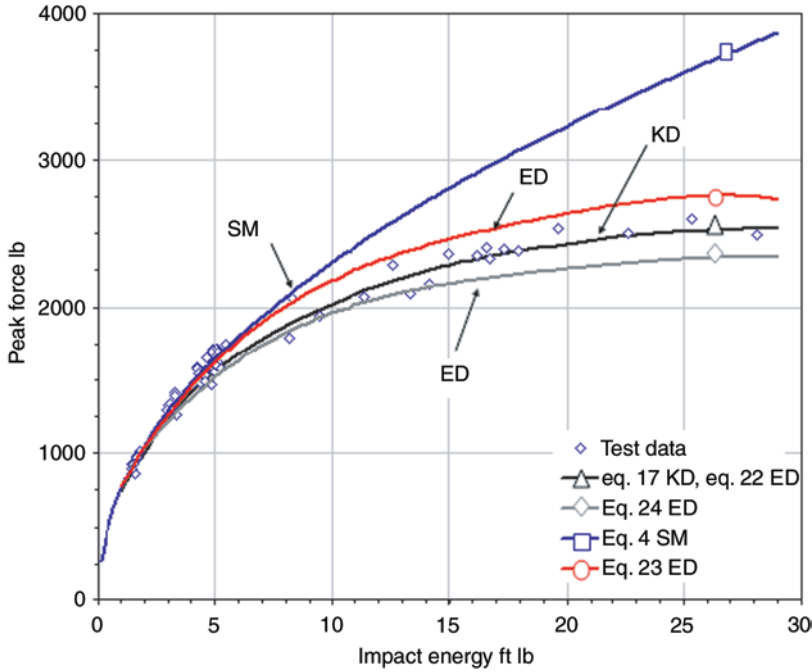


Figure 10. Damaged stiffness and dissipated energy model predictions for configuration C1.

unmodified (K_0), it is then possible to substitute the nominal impact energy (E_i) of Equation (4) with the effective impact energy (E_i^*), where:

$$E_i^* = E_i - E_D. \tag{21}$$

As in the case of Equation (17), it is necessary to employ a ratio of time-to-failure against time-to-peak-force to separate the force–time trace into segments, and to make the individual terms nondimensional (Figure 9). For the first segment (before the onset of damage), the energy dissipated is assumed to be negligible, and the entire available kinetic energy contributes in achieving the theoretical value of peak force.

$$P_{ED}^{peak} = \sqrt{2K_0 \left[\left(\frac{t_{f1}}{t_M} \right) E_i + \left(\frac{t_{f2} - t_{f1}}{t_M} \right) (E_i^{*j}) + \dots + \left(\frac{t_M - t_f}{t_M} \right) (E_i^{*M}) \right]} \tag{22}$$

where $E_i^{*j} = E_i - E_D^j$ and $j = (1-M)$ as in Equation (16). This type of approach proves to be as accurate as the one of Equation (17), but has the disadvantage that the instantaneous value of the energy dissipated is not as readily available as the structural stiffness K_D . A simplification can then be made, and instead of dividing the curve into multiple individual segments, it is divided only into two regions, before and after failure:

$$P_{ED}^{peak} = \sqrt{2K_0 \left[\left(\frac{t_{f1}}{t_M} \right) E_i + \left(\frac{t_M - t_f}{t_M} \right) (E_i^{*M}) \right]} = \sqrt{2K_0 \left[E_i - \left(\frac{t_M - t_f}{t_M} \right) E_D \right]} \tag{23}$$

where the symbols bear the same significance as in previous equations. The great advantage of this simplified model is that only the values of t_f and E_D (total energy dissipated, plotted in Figure 3, which is simply a fraction of E_i) need to be determined, therefore minimal experimental correlation is required. However, this model tends to slightly overestimate the effective result (Figure 10, Equation (23)), mostly because it assumes that energy is not dissipated in the elastic regime. In practice, it has been shown (Figures 1 and 3) that a small yet measurable portion of energy is absorbed in a nonconservative phenomena even in the elastic regime, as stated by Equation (5). To further simplify the energy dissipated model, an assumption is made that the entire energy dissipated in the fracture process does not contribute to increasing the peak recorded force. In other words, that the entire amount of E_D is dissipated at the beginning of contact ($t_f=0$), hence:

$$P_{ED}^{\text{peak}} = \sqrt{2K_0(E_i - E_D)}. \quad (24)$$

The great advantage of this equation is that E_D , which is the only additional unknown with respect to Equation (4), is often readily available (or can easily be calculated) from an impact test [3,6]. On the other hand, this equation tends to slightly underestimate the actual value of the peak force (Figure 11, Equation (24)), since, only part of the damage process occurs during the loading part of the curve, while the other part of it occurs after reaching peak force.

Spring–Mass–Dashpot (SMD) Model

The SMD model embodies a nonlinear viscous damper for capturing the effect of damage on the transient response of a panel subjected to low-velocity impact. The choice of employing a nonlinear viscous damper rather than a nonlinear spring to model damage is related to the nature of the event itself. In the case of a quasi-static indentation test [11,12,21,22], the use of a nonlinear spring (displacement-proportional) to model the load–deflection response of the plate after damage has solid physical significance. On the other hand, the dynamic nature of the impact event is such that it lends itself to energy-proportional (nonlinear velocity) interpretation. Herein lays the fundamental difference with previous models. Furthermore, the nonlinear damper is proportional to the energy absorbed in the event, and not simply the incident kinetic energy, thereby adding a strong physical support to this model. On the other hand, the model is now a function of two additional unknowns, which have to be determined empirically. Let us now set:

$$m\ddot{x} + c\dot{x}^n + kx = 0 \quad (25)$$

where c and n are the damping coefficient and damping exponent respectively, while the other symbols have the same significance of Equation (1). One can also rewrite:

$$P = K_0x - cV^n \quad (26)$$

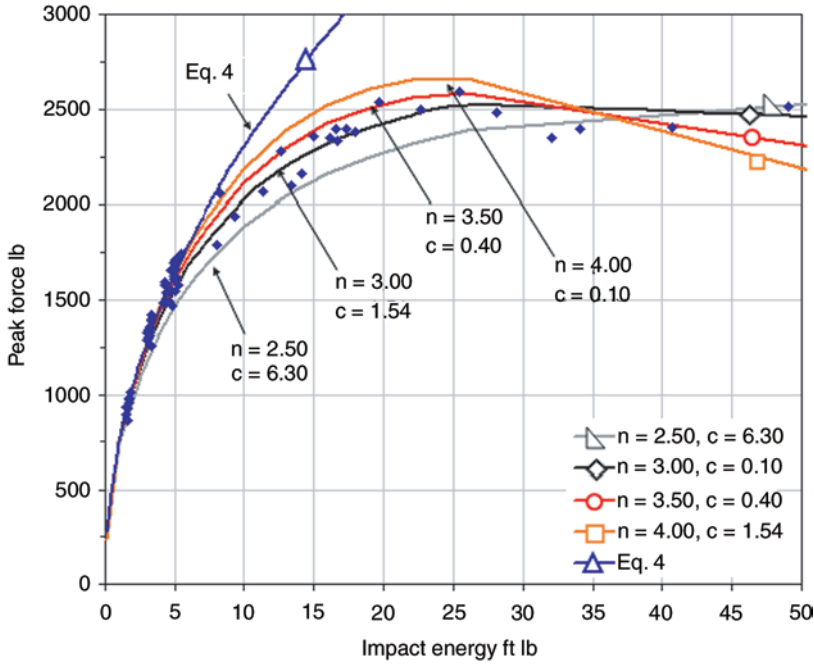


Figure 11. SMD predictions for configuration 1 using four combinations of the c and n parameters.

where P is the instantaneous value of the contact force. Considering the system to be elastic (only a mathematical expedient), it is possible to apply the following energy balance:

$$U = \frac{1}{2} P^{\text{peak}} x^{\text{max}} = E_i \tag{27}$$

where U is the work done in displacing the panel up to max deflection x^{max} where the force reaches the value of P^{peak} . This energy balance assumes that the internal deformation work done by the panel coincides with the available kinetic energy, without including any losses due to the non-conservative phenomena, which is known to be only an approximation (Equation (5)), but helps greatly in the mathematical derivation. It is then possible to obtain:

$$P_{\text{SMD}}^{\text{peak}} = \frac{1}{2} \left(-cV^n + \sqrt{c^2V^{2n} + 8K_0E_i} \right) = -\frac{c}{2}V^n + \sqrt{2K_0E_i + \frac{c^2V^{2n}}{4}} \tag{28}$$

which holds true in both the sub-critical and super-critical regimes, since for $c=0$ (no damage) it reduces to Equation (4).

The results of applying the SMD model to the reference configuration C1 are shown in Figure 11. The choice of the empirical parameters c and n is all but arbitrary. The damping exponent n falls somewhere in the range 2.5–4.0 (Equation (20)), and the value of the damping coefficient c is strictly related to the value selected for n . In particular, c and n are inversely related, and have different effects on the shape of the force–energy curve.

Low values of n (e.g., 2.5, 3.0) are characterized by low values of the peak force in the sub-critical and early super-critical regions. However, they lead to very accurate asymptotic values in the dynamic plateau region. On the other hand, high values of n (e.g., 3.5, 4.0) tend to give accurate predictions of the peak force in the early portions of the curve, but fall greatly below the experimental data points in the dynamic plateau region. Furthermore, for a specific value of n , it is possible to obtain a value of c by integrating the equation:

$$E_D = \int c\dot{x}^n dx \quad (29)$$

between $0-x^{\max}$, knowing the quantity of E_D from the impact test data. The physical meaning of Equation (29) is that the total work done by the viscous force associated with the damper representing damage is equal to the total energy dissipated during the impact event.

For configuration C1, the most accurate model features values of $c = 1.54$ and $n = 3.00$ (Figure 11). The validity of the model can however be extended to all other structural configurations considered in this investigation (Table 1), and the results are shown in Figure 12. More flexible configurations (e.g., C2, C3) exhibit lower values of damping coefficient c than stiffer configurations (e.g., C5) for the same value of damping exponent n . The coefficient c is a measure of how much damage is created, while the exponent n is an indication of how much this damage depends on the severity of the impact event. For that reason stiffer configurations are much more sensible to the presence of damage (from a dynamic response standpoint only!) than flexural-dominated configurations. For all configurations considered, a value of n around 3.0 has shown to give the most accurate predictions. Setting then $n = 3.0$, the value of c for configurations C1, C3–C5 is shown to be a function of the laminate thickness t :

$$c = \alpha t^\beta \quad (30)$$

where $\alpha = 19.3$ and $\beta = 1.32$. It is then possible to derive design curves, such as the ones in Figure 13, which relate different values of c and n and allow for extrapolation to other structural configurations.

CONCLUSIONS

The limitations associated with the use of a spring–mass model to describe the impact response of composite panels have been demonstrated. Modifications were suggested that retained the simple formulation of the spring–mass model while allowing for the inclusion of the effect of damage on the transient response, thereby greatly improving the prediction of peak contact force. Each of the three models developed (damaged stiffness, dissipated energy, and Spring–Mass–Dashpot) introduces additional unknowns that need to be empirically determined, but have a solid physical foundation. Every model offers its own advantage, but in general the greater the accuracy, the more the empirical correlation required.

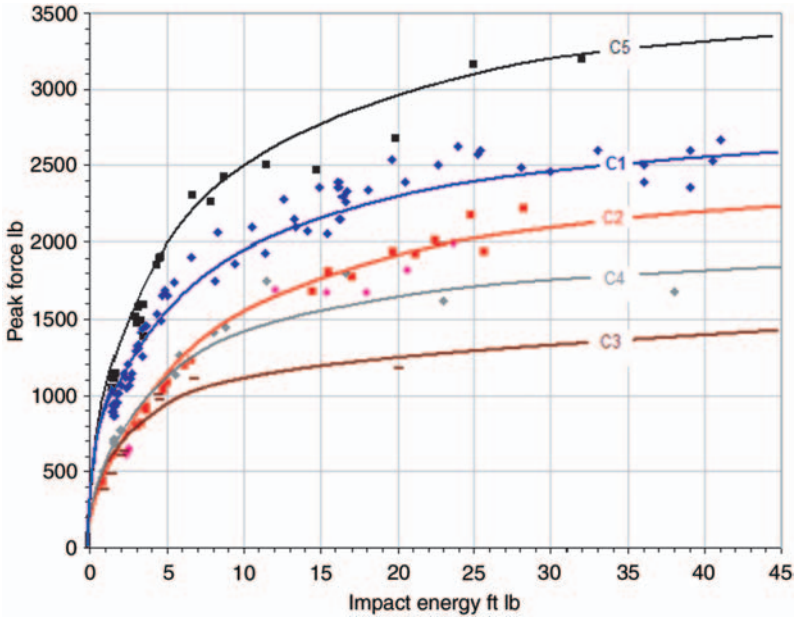


Figure 12. Force–energy plot for all five structural configurations, showing experimental data points and SMD predictions.

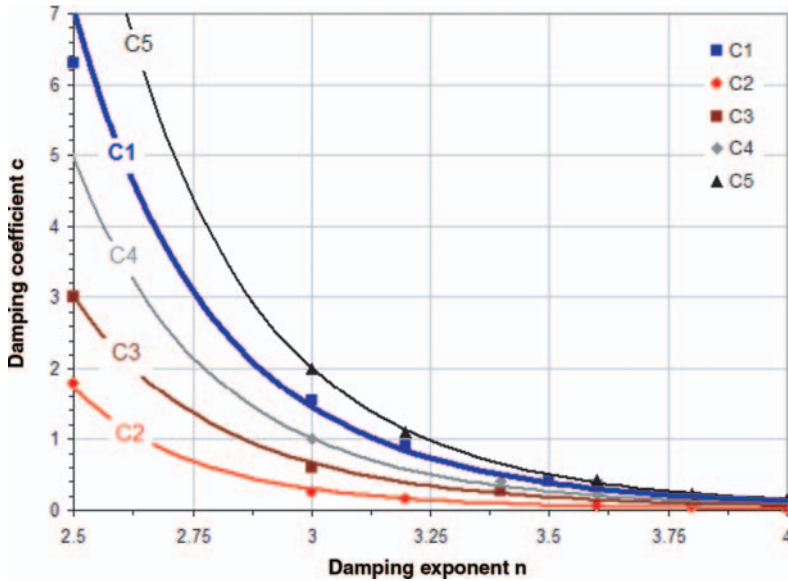


Figure 13. Design curves for combination of c - n parameters for all five structural configurations.

ACKNOWLEDGMENTS

The author would like to express his gratitude to his eternal advisor Keith T. Kedward (University of California, Santa Barbara), T. Kevin O'Brien (Army Research Laboratories

at NASA Langley), C.T. Sun (Purdue University), Bhavani Sankar (University of Florida), John Bruch, Jr. (University of California, Santa Barbara), and Dan Jacobson (SD Composites) for the valuable comments over the years, which contributed to improve the quality of this work. *Per aspera astra ad ulteriora.*

REFERENCES

1. Kan, H.P. and Graves, M.J. (1988). Damage Tolerance of Composites, Vol. III: Analysis, Methods, Development, and Test Verification, Air Force Wright Aeronautical Laboratories, AFWAL-TR-87-3030, July 1988.
2. Kan, H.P., Cordero, R. and Whitehead, R.S. (1997). Advanced Certification Methodology for Composite Structures, DOT/FAA/AR-96/111, April 1997.
3. Ireland, D.R. (1974). Procedures and Problems Associated with Reliable Control of Instrumented Impact Test, *Instrumented Impact Testing*, ASTM STP 563, pp. 3–29.
4. Jackson, W.C. and Poe, Jr., C.C. (1993). The Use of Impact Force as a Scale Parameter for the Impact Response of Composite Laminates, *Journal of Composites Technology and Research*, Winter, **15**(4): 282–289.
5. Shivakumar, K.N., Elber, W. and Illg, W. (1985). Prediction of Impact Force and Duration due to Low-velocity Impact on Circular Composite Laminates, *Journal of Applied Mechanics*, **52**: 674–680.
6. Feraboli, P. and Kedward, K.T. (2004). Enhanced Evaluation of the Low-velocity Impact Response of Composite Plates, *AIAA Journal*, **42**(10): 2143–2152.
7. Ambur, D.R., Prasad, C.B., Rose, C.A., Feraboli, P. and Jackson, W.C. (2005). Scaling the Non-linear Impact Response of Flat and Curved Composite Panels, In: *46th AIAA Structures, Structural Dynamics and Materials Conference*, April 2005, pp. 2005–2224.
8. Feraboli, P., Jackson, W.C. and Rose, C.A. (2006). Damage Resistance Characteristics of Very-thick-core Honeycomb Sandwich Panels, In: *47th AIAA Structures, Structural Dynamics and Materials Conference*, April 2006.
9. Nettles, A.T. and Douglas, M.J. (2000) A Comparison of Quasi-static Indentation to Low-velocity Impact, NASA TP 210481, August 2000.
10. Tomblin, J., Raju, Suresh K. and Arosteguy, G. (2004). Damage Resistance and Tolerance of Composite Sandwich Panels – Scaling Effects, DOT/FAA AR-03/75, Feb. 2004.
11. Tomblin, J.S. and Raju, K.S. (2001). Damage Characteristics in Sandwich Panels Subjected to Static Indentation using Spherical Indentors, In: *42nd AIAA Structures, Structural Dynamics, and Materials Conference*, Paper 2001-1189.
12. Abrate, S. (2001). Modeling of Impacts on Composite Structures, *Composite Structures*, **51**: 129–138.
13. Cawley, P. and Adams, R.D. (1979). A Vibration Technique for Non Destructive Testing of Fibre Composite Structures, *J. Composite Materials*, **13**: 161–175.
14. Delfosse, D. and Poursartip, A. (1997). Energy-based Approach to Impact Damage in CFRP, *Composites Part A*, **28A**: 647–655.
15. Hinrichs, S., Chen, V., Jegley, D., Dickinson, L.C. and Kedward, K. (1995). Effect of Impact on Stitched/RFI Compression Panels, In: *Fifth NASA/DoD Advanced Composites Technology Conference*, NASA CP 3294 Vol. I Part 2, May 1995, pp. 879–912.
16. Olsson, R., Asp, L.E., Nilsson, S. and Sjogren, A. (2000). A Review of Some Key Development in the Analysis of the Effects of Impact upon Composite Structures, ASTM STP 1383, 12–28.
17. Johnson, S.H. and Lieberman, B.B. (1996). Normal Impact Models for Golf Balls, In: *1st International Conference on the Engineering of Sport*, pp. 251–256.
18. Goldsmith, W. (1960). *Impact*, Edward Arnold.

19. Cochran, A.J. (1998). Club Face Flexibility and Coefficient of Restitution, In: *Proceedings of the 3rd World Scientific Congress of Golf*, pp. 486–492.
20. Gong, S.W. and Lam, K.Y. (2000). Effects of Structural Damping and Stiffness on Impact Response of Layered Structure, *AIAA Journal*, 38/9, September 2000, pp. 1730–1735.
21. Anderson, T.A. (2005). An Investigation of SDOF Models for Large Mass Impact on Sandwich Composites, *Composites: Part B*, **36**: 135–142.
22. Hoo-Fatt, M.S. and Park, K.S. (2001). Dynamic Models for Low Velocity Impact Damage of Composite Sandwich Panels, Part A: Deformation, *Composite Structures*, **52**: 335–351.

BIOGRAPHY

Paolo Feraboli

Paolo Feraboli joined the Department of Aeronautics and Astronautics of the University of Washington in the summer of 2005 as Assistant Professor in Aerospace Structures and Materials. Previously, he was a visiting researcher at NASA Langley Research Center in the Mechanics and Durability Branch. He earned his PhD from the University of California at Santa Barbara under the supervision of Dr Keith T. Kedward, and holds previous degrees in Mechanical Engineering from the University of Bologna, Italy. His major areas of interests are aircraft safety certification and composite structures design for damage resistance and tolerance. He has authored over 20 publications between peer-reviewed journals and internationally acclaimed conferences. He is the chairman of the MIL-HDBK-17 Work Group on Crashworthiness, and an active member of AIAA, SAMPE, and ASC. Prior to joining UCSB, he worked for Automobili Lamborghini S.p.A. in Sant'Agata Bolognese, where he was involved with the development of innovative primary composite structures for the Murcièlago lineup, and contributed to the development of an all-carbon-composite door for crash certification.